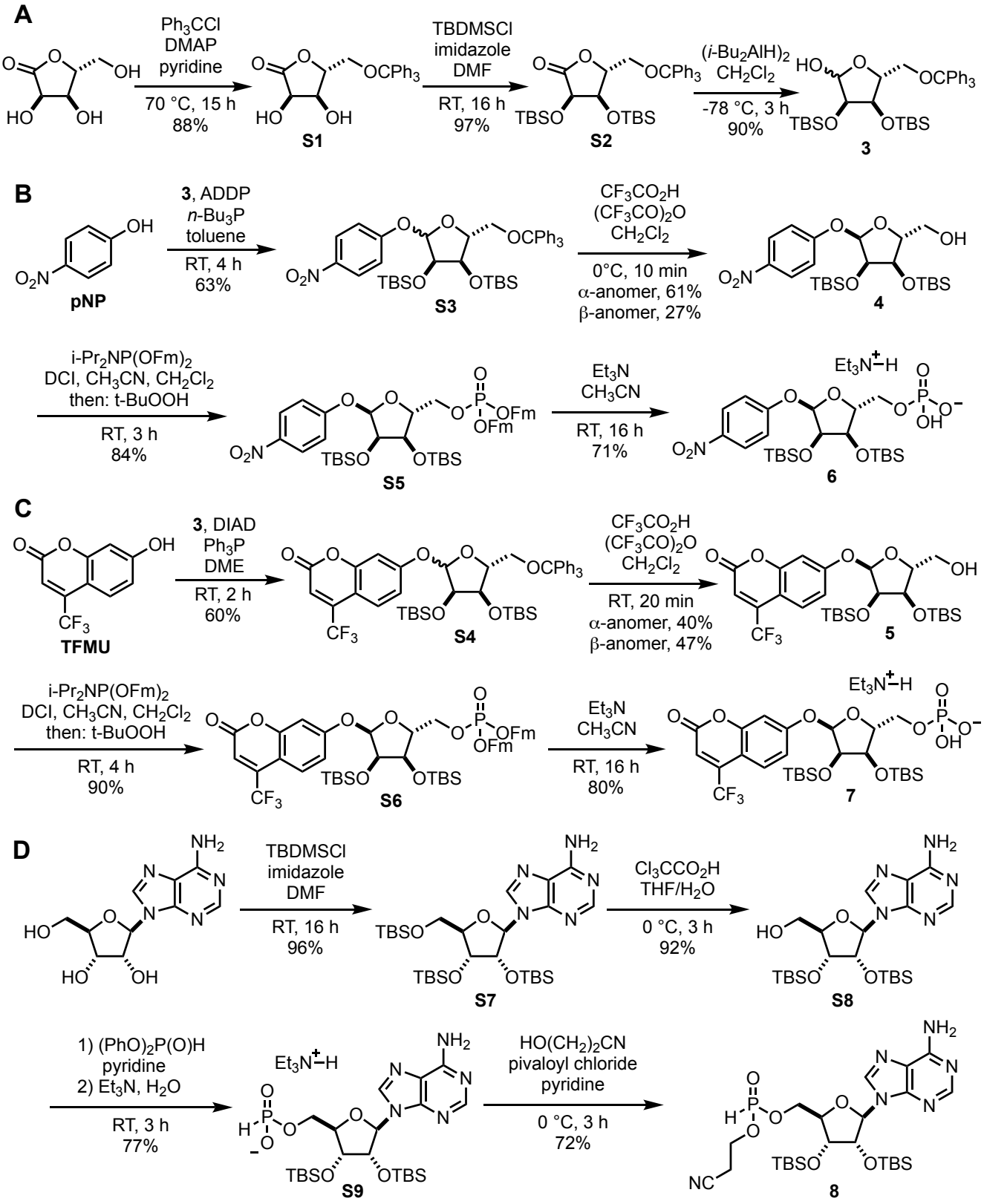

Figure S1: Related to Figure 2. Expanded synthetic scheme of glycosyl donor (A), pNP-ribose (B), TFMU-ribose (C), and adenosine phosphonate (D).

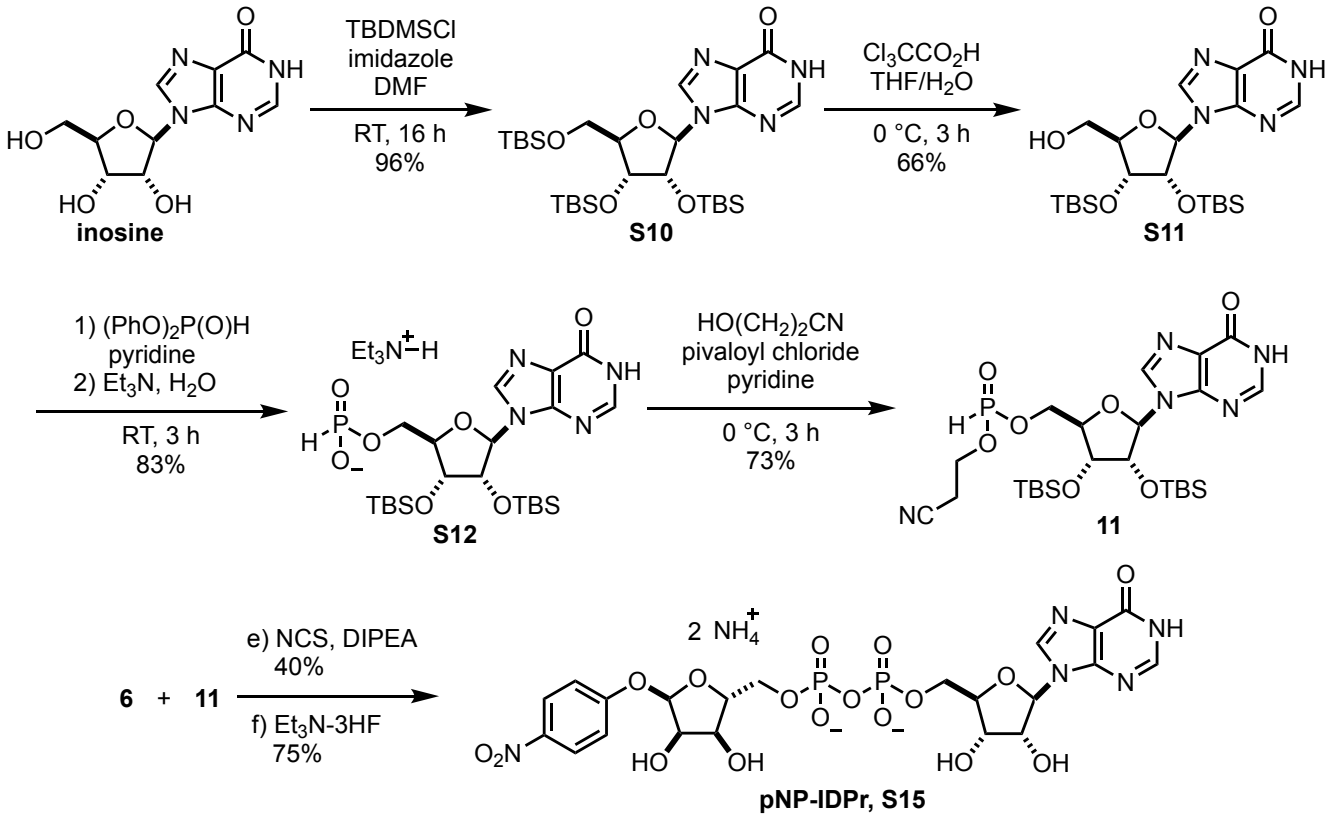

Figure S2: Related to Figure 3. Synthesis of pNP-IDPr.

Table S1: Related to Figure 3. Docking scores for sugar nucleotides in PARG and ARH3.

Enzyme	Ligand	SP score (kcal/mol)	SP Difference (kcal/mol)	XP score (kcal/mol)	XP difference (kcal/mol)
L. chalumnae ARH3	ADPr	-7.539	-	-6.254	-
	IDPr	-6.729	0.810	-7.000	-0.746
	GDPr	-6.692	0.847	-6.131	0.123
	XDPr	-7.100	0.439	-6.732	-0.478
H. sapiens PARG	ADPr	-12.229	-	-8.262	-
	IDPr	-10.332	1.897	-6.613	1.649
	GDPr	-10.906	1.323	-6.323	1.939
	XDPr	-11.292	0.937	-6.090	2.172

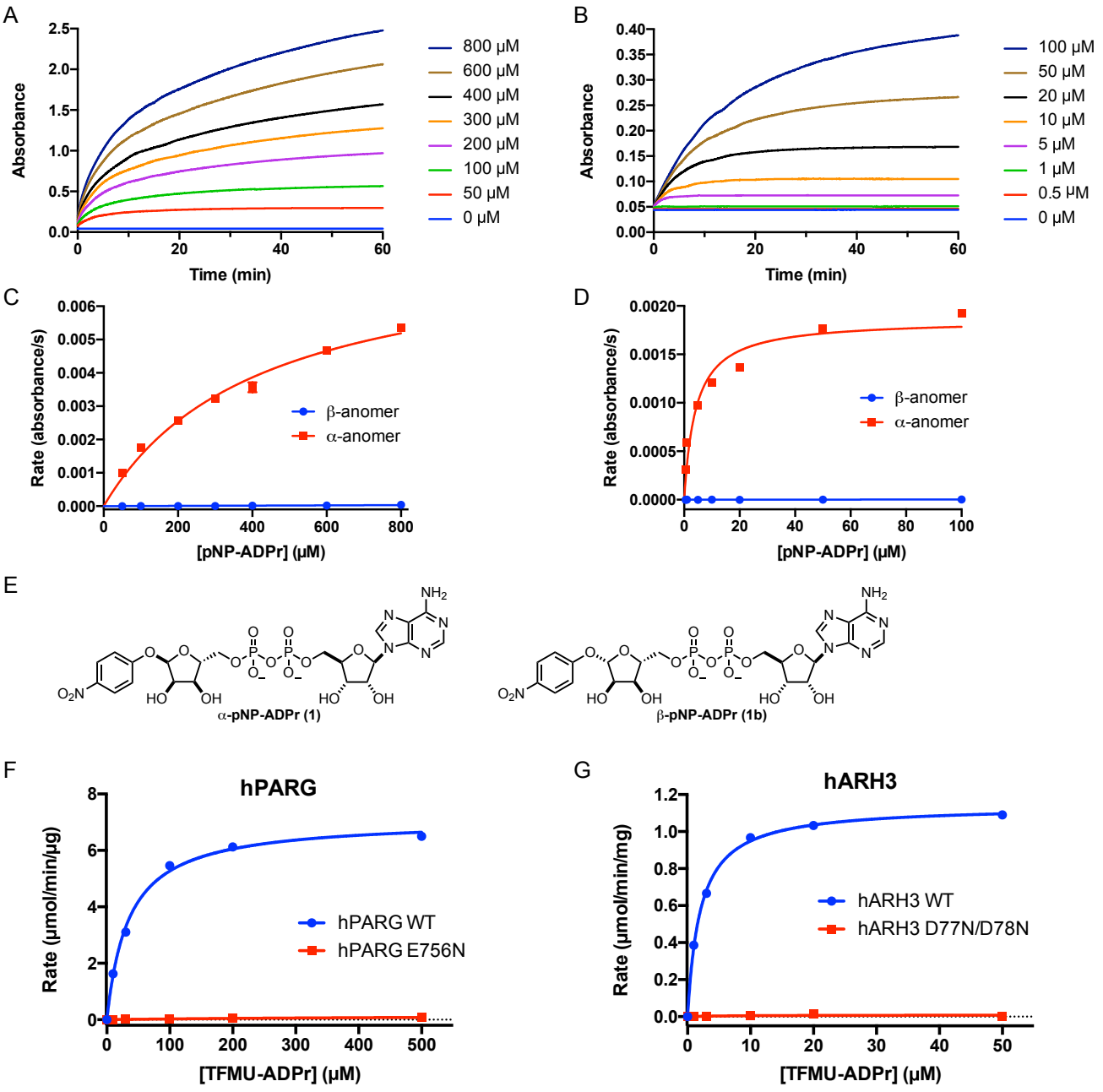

Figure S3: Related to Figure 4. A. Reaction progress curves of ttPARG-catalyzed hydrolysis of **pNP-ADPr**. Enzyme (50 nM) was incubated with varying concentration of **pNP-ADPr** in 50 µL of appropriate reaction buffer in a 384-well plate. Reaction was monitored every 2 s for 60 min. B. Same as B but with hARH3. C. Stereoselectivity of PARG and ARH3 for α glycosidic bonds. ttPARG (50 nM) was incubated with varying concentrations of α and β **pNP-ADPr** in 50 µL of appropriate reaction buffer in a 384-well plate. Initial reaction rates were obtained by monitoring reaction progress using an absorbance plate reader (405 nm). D. Same as C but with hARH3. E. Structures of α and β **pNP-ADPr**. F. Processing of TFMU-ADPr by catalytically active (WT) and inactive (E756N) hPARG. G. Processing of TFMU-ADPr by catalytically active (WT) and inactive (D77N/D78N) hARH3. Error bars represent SEM, n = 3.

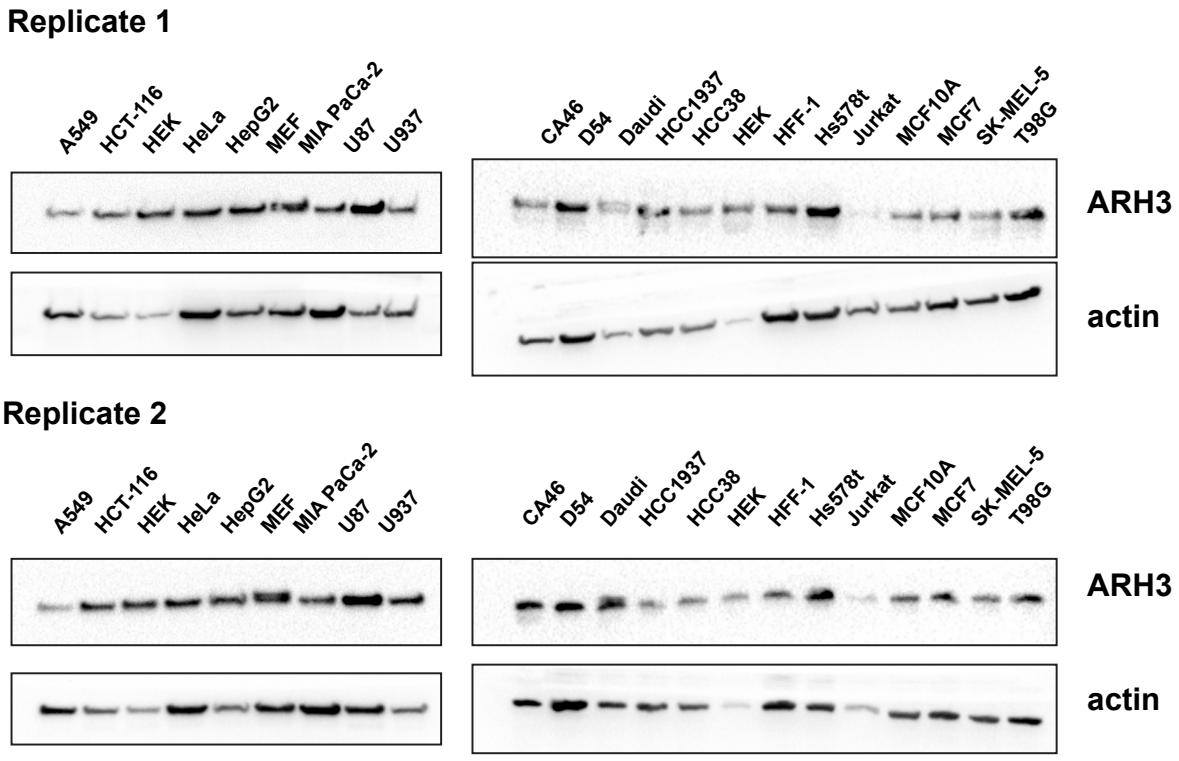

Figure S4: Related to Figure 5. Expanded images of Western blotting to evaluate ARH3 expression. Replicate 1 is same as shown in Figure 5D but without straightening. Anti-ARH3 (1:1000), anti-PARP1 (1:3000), anti-actin (1:3000).

Table S2: Related to Figure 5. Data used to construct Figure 5D.

Cell Line	ARH3 Activity (milli-units/min/μg)	Relative ARH3 expression (ARH3/actin)
U87	290±52	2.3±0.4
HepG2	215±19	3.0±0.9
HEK	192±20	3.3±0.4
HCT-116	173±17	1.54±0.06
Hs578t	170±34	1.5±0.6
HeLa	159±18	1.0±0.2
MIA PaCa-2	157±25	0.49±0.08
MEF	153±38	1.24±0.09
D54	147±34	0.90±0.05
T98G	139±7	0.9±0.2
U937	137±34	1.0±0.3
HFF-1	105±20	0.5±0.1
HCC38	100±19	0.88±0.09
MCF7	92±40	0.8±0.3
SK-MEL-5	87±13	0.7±0.2
HCC1937	76±4	0.9±0.2
A549	67±23	0.38±0.02
Jurkat	36±7	0.3±0.2
Daudi	27±35	1.6±0.7
MCF10A	-5±12	0.8±0.3

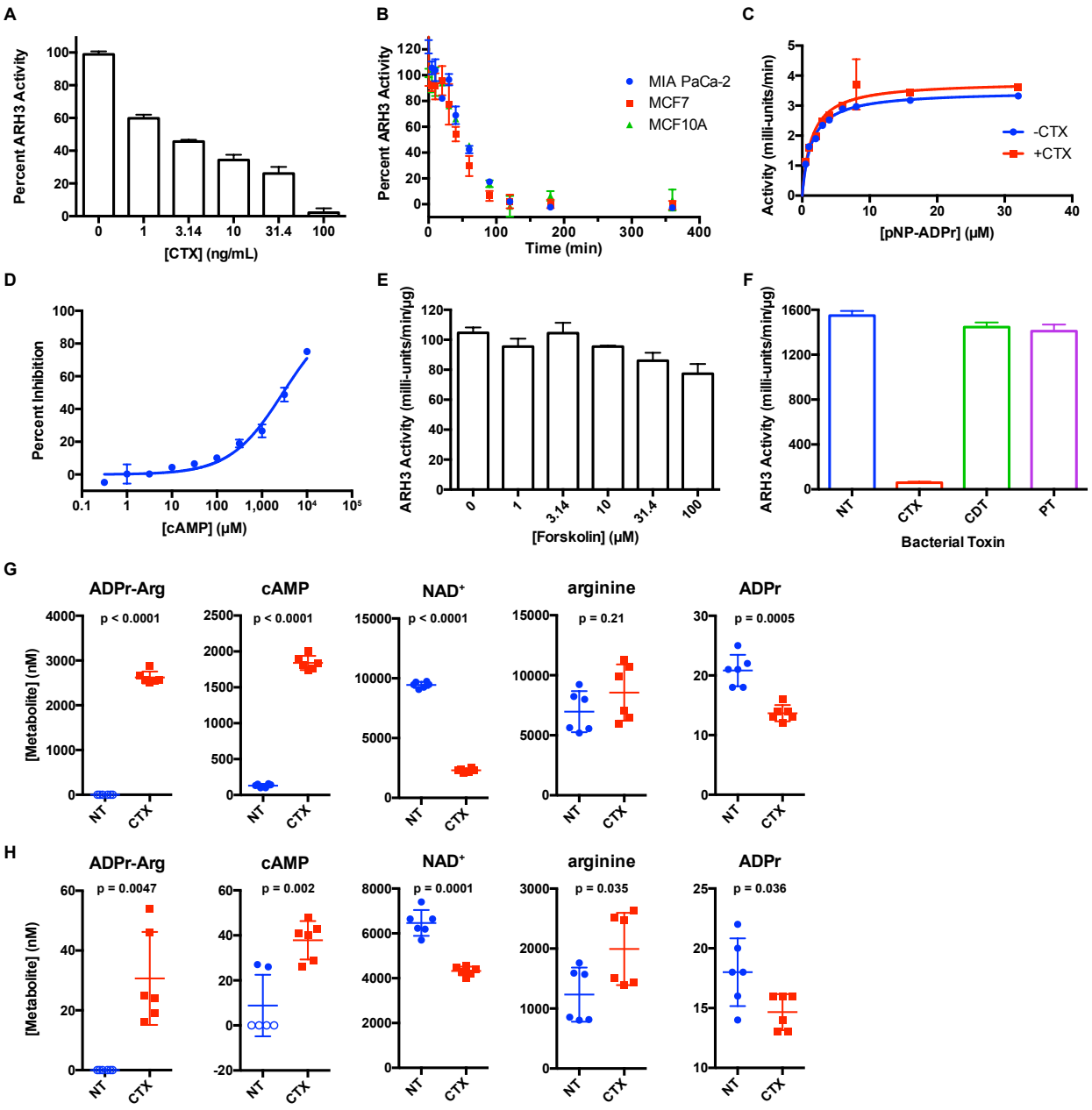

Figure S5: Related to Figure 6. A. MCF10A cells were cultured in the absence of CTX for five passages. Cells were plated 1x10^5 cells/well in 6-well plate. Cells were treated with varied concentration of CTX for 48 h. Remaining ARH3 activity was measured with 200 μM **TFMU-IDPr**. B. Cells were plated 3x105 cells/well in 6-well plate. Cells were treated with 100 ng/mL CTX for the indicated period of time. Remaining ARH3 activity was measured with 200 μM **TFMU-IDPr**. C. In vitro activity of purified ARH3 in the presence or absence of 100 ng/mL CTX. D. Dose-response curve of ARH3 inhibition by cAMP using 200 μM TFMU-IDPr. E. MCF10A cells treated with forskolin for 1 h. F. A549 cells treated with various bacterial toxins for 24 h. Following treatment, ARH3 activity in cell lysate was assessed. CTX, cholera toxin 100 ng/mL; CDT, *C. difficile* toxin 200 ng/mL CDTa 400 ng/mL CDTb; PT, pertussis toxin 100 ng/mL. G. Metabolic profiling of MCF7 cells treated with 100 ng/mL CTX for 6 h. Metabolites (ADPr-Arg, cAMP, ADP-ribose, NAD$^+$, and arginine) in methanolic cell extract were quantified by LC-MS/MS. Samples below the limit of detection are indicated by open points. Error bars represent standard deviation, n = 6. P values are from unpaired t-test with Welch's correction H. Same as G but with U2OS cells.

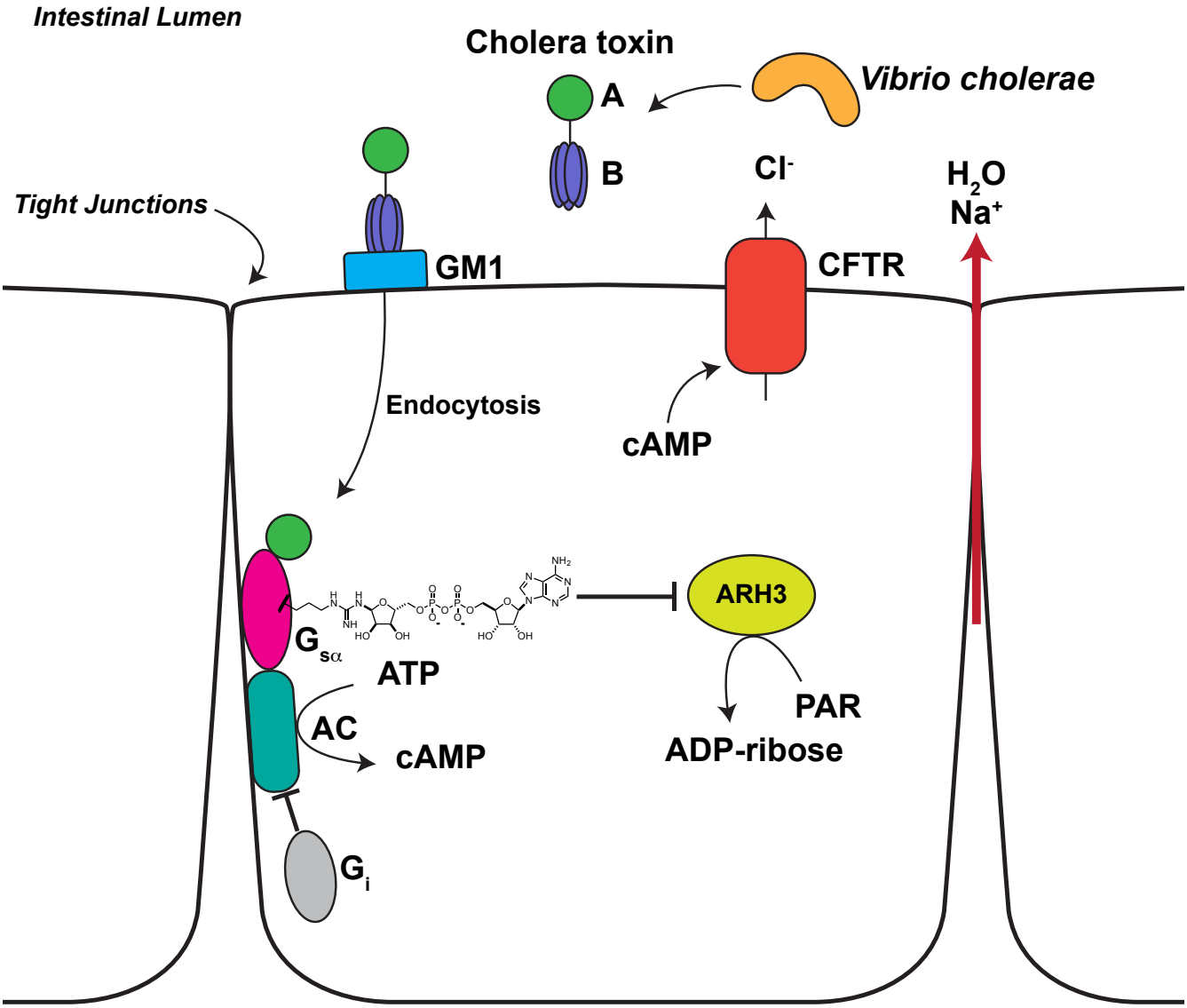

Figure S6: Related to Figure 6. Canonical mechanism of action for cholera toxin and involvement of ARH3. Cholera toxin is secreted as a binary toxin by *Vibrio cholera* within the intestinal lumen. Subunit B binds to GM1 receptor and is endocytosed. Subunit A contains an ADP-ribosyltransferase domain that ADP-ribosylates $G_{s\alpha}$. This PTM causes constitutive activitation of $G_{s\alpha}$, which activates AC leading to cAMP synthesis. Increased cAMP concentrations lead to cystic fibrosis transmembrane conductance regulator (CFTR) activation and efflux of chloride. Tight junctions are weakened leading to sodium and water leakage through the intercellular space, resulting in dehydration and loss of electrolytes (Thiagarajah and Verkman, 2012). Pertussis toxin acts through a similar manner by ADP-ribosylation of G_i which also gives rise to increased cAMP synthesis.